Earth and Planetary Science Letters 302 (2011) 60–70

Contents lists available at ScienceDirect

Earth and Planetary Science Letters

journal homepage: www.elsevier.com/locate/epsl

A note of caution on the use of boulders for exposure dating of depositional surfaces

Silke Schmidt [a,*], Ralf Hetzel [a], Jan Kuhlmann [a], Francisco Mingorance [b], Victor A. Ramos [c]

[a] Institut für Geologie und Paläontologie, Westfälische Wilhelms-Universität Münster, Corrensstraße 24, Münster, 48149, Germany
[b] Instituto de Mecánica Estructural y Riesgo Sísmico, Universidad Nacional de Cuyo, Casilla de Correo 405, Correo Central, Mendoza, 5500, Argentina
[c] Laboratorio de Tectónica Andina, Universidad de Buenos Aires, Ciudad Universitaria, Pabellón II, Buenos Aires, 1428, Argentina

ARTICLE INFO

Article history:
Received 9 August 2010
Received in revised form 22 November 2010
Accepted 23 November 2010
Available online 22 December 2010

Editor: T.M. Harrison

Keywords:
^{10}Be exposure dating
inherited nuclide component
amalgamation approach
fluvial terraces
Andean Precordillera

ABSTRACT

Exposure dating of boulders has been widely applied to determine the age of depositional surfaces under the assumption that the pre-depositional nuclide component in most boulders is negligible. Here we present a case study on fluvial terraces at the active mountain front of the eastern Andes, where this assumption is clearly invalid, because sandstone boulders ($n=13$) from terraces at two sites contain a highly variable inherited ^{10}Be component and have apparent ^{10}Be ages that exceed the age of the respective surface by up to ~90 ka. Likewise, boulders from active stream channels ($n=5$) contain a substantial inherited ^{10}Be component, equivalent to 5–48 ka of exposure. The age of the fluvial terraces is well determined by two approaches that allow to correct for the pre-depositional nuclide component: ^{10}Be dating of amalgamated pebbles and ^{10}Be depth profiles on sand samples. At site 1, three terraces have ^{10}Be ages of 3–5 ka (T_2), 11–13 ka (T_3), and 16–20 ka (T_4), which are consistent with the terrace stratigraphy. The age of terrace T_3 is confirmed by a calibrated ^{14}C age of 12.61 ± 0.20 ka BP obtained from a wood sample. At site 2, terrace T_3 has a ^{10}Be age of 13–16 ka. The average inherited ^{10}Be concentration of sand grains – determined from depth profiles and stream sediments – is small and equivalent to 1–3 ka of exposure. In contrast, the mean inheritance of pebbles and boulders is higher and equivalent to exposure times of ~10 ka and ~30 ka, respectively. These differences in the pre-depositional nuclide component are related to the different provenance and transport history of sand, pebbles, and boulders. The sand is derived from rapidly eroding Miocene sediments exposed near the mountain front, whereas the pebbles and boulders originate from Triassic sandstones in the internal part of the fold-and-thrust belt. On their way to the mountain front, boulders and pebbles were temporarily stored and irradiated in alluvial fans that are currently reworked. As sediment deposition in intramontane basins and their subsequent excavation is common in the Andes and other fold-and-thrust belts, the presence of pre-depositional nuclide components should be evaluated when applying exposure dating at active mountain fronts.

1. Introduction

Exposure dating of depositional surfaces using *in situ*-produced cosmogenic nuclides is an important tool in geomorphology and can, for instance, be used to quantify slip rates of active faults (e.g. Gold et al., 2009; Hetzel et al., 2002; van der Woerd et al., 1998), determine rates of river incision (e.g. Burbank et al., 1996; Hetzel et al., 2006), date phases of rapid alluviation (e.g. Hein et al., 2009; Pratt et al., 2002), or constrain periods of debris flow activity (e.g. Dühnforth et al., 2007). When dating depositional surfaces such as river terraces or alluvial fans it is necessary to take into account that cosmogenic nuclides are not only produced after formation of the respective surfaces, but also during erosion of the host rock and sedimentary transport of clasts. This pre-depositional nuclide component, also known as inherited component, must be determined or, alternatively, it must be shown that it is negligible.

To quantify the pre-depositional nuclide component Anderson et al. (1996) introduced an approach that is based on the amalgamation of many clasts into one sample. This amalgamation averages the inherited components of the individual clasts, which result from their different exhumation and transport histories. Numerical modeling by Hancock et al. (1999) has shown that at least 30 clasts are required to reduce the standard deviation of the inherited component to 20%. At least two samples are required to apply the amalgamation approach: a surface sample and a sample from the subsurface, which is typically taken at a depth of 1–2 m. The different nuclide concentrations of these two samples, which result from the attenuation of the cosmic rays with depth, can be used to quantify both the inheritance of the sediment and the exposure age of the alluvial surface, if the surface has not been eroded (Anderson et al., 1996). The amalgamation approach assumes that the inherited nuclide component over the sampled depth interval is constant, which is difficult to demonstrate

* Corresponding author. Tel.: +49 251 83 33 989; fax: +49 251 83 33 933.
E-mail address: silkeschmidt@uni-muenster.de (S. Schmidt).

0012-821X/$ – see front matter © 2010 Elsevier B.V. All rights reserved.
doi:10.1016/j.epsl.2010.11.039

from just two samples. Therefore, subsequent studies used several subsurface samples to obtain depth profiles (e.g. Guralnik et al., 2011; Hancock et al., 1999; Hetzel et al., 2002; Phillips et al., 1998; Repka et al., 1997). If the sediment had indeed a constant nuclide concentration with depth at the time of deposition, measured nuclide concentrations will follow the shifted exponential equation

$$C(z) = C_i + C_s \exp(-\mu z), \quad (1)$$

where $C(z)$ is the nuclide concentration C at a depth z, C_i is the inherited nuclide concentration, C_s is the post-depositional nuclide concentration at the surface of the deposit, and μ is the absorption coefficient defined as $\mu = \rho/\Lambda$, where ρ is the density and Λ the effective attenuation length of the secondary neutrons (Hancock et al., 1999; Lal, 1991; Phillips et al., 1998). Note that this equation does not account for the decay of radionuclides, which is justified if the age of the surface is small relative to the half-life. It also neglects the subordinate production of cosmogenic nuclides by muons. For surfaces that are relatively old or have been significantly eroded the nuclide production by negative and fast muons should be taken into account (for details see Braucher et al., 2009; Hein et al., 2009; Schaller et al., 2010; Siame et al., 2004). Instead of using depth profiles, another more simple way of estimating the inherited nuclide component is to analyze sediment from active channels (Hancock et al., 1999; Hetzel et al., 2002; Repka et al., 1997). However, this approach requires that the stream sediments have the same nuclide concentration as the sediments deposited during the formation of the surfaces. This assumption may be incorrect because rates of erosion and sediment transport can vary through time, in particular over glacial–interglacial cycles (e.g. Meyer et al., 2010; Schaller et al., 2004).

Exposure dating of individual boulders or cobbles is another way to determine the age of depositional surfaces (e.g. Bierman et al., 1995; Brown et al., 2002; Siame et al., 1997; van der Woerd et al., 2006). If several boulders from the same surface yield exposure ages that are identical within their error, it is likely that the boulders contain only a negligible inherited component. Indeed, a tight clustering of ages has been documented by several studies, although a few boulders (or cobbles) may yield older ages (Bierman et al., 1995; Kirby et al., 2006; Palumbo et al., 2009; Ritz et al., 2003; Siame et al., 1997; Zehfuss et al., 2001). The latter are considered as outliers with a significant inherited component (e.g. Brown et al., 2002; van der Woerd et al., 1998). The fact that many boulders and cobbles have a negligible pre-depositional component likely results from the rapid erosion of their source area, for example by intense glacial activity or repeated landsliding, and a short transport time in the channel network (e.g. van der Woerd et al., 1998). Especially boulders from moraines often yield narrow age clusters thus indicating a negligible inherited component (e.g. Kaplan et al., 2010; Mériaux et al., 2009; Phillips et al., 1997; Schaefer et al., 2009).

In this study we apply exposure dating of boulders and the amalgamation approach on sand samples and pebbles to date fluvial terraces at the mountain front of the Andean Precordillera with cosmogenic ^{10}Be in quartz. Our results show that 17 of 18 boulders have a significant inherited component, which precludes their use for exposure dating. In contrast, sand samples from depth profiles and amalgamated pebbles yield stratigraphically consistent exposure ages for the terraces.

2. Geology of the study area in the eastern Andes

The Andean Precordillera is a north–south trending fold-and-thrust belt that constitutes the easternmost mountain range of the Andes between 28° and 33° S (Ramos et al., 2002; Vergés et al., 2007). In the southern part of the Precordillera, north of Mendoza, sediments of Triassic to Ordovician age are exposed in the hanging wall of the inactive Higueras thrust (Fig. 1a; Ahumada et al., 2006; Sepúlveda, 2001). At the mountain front farther east, Miocene sediments are thrust upon Late Quaternary sediments by the tectonically active Peñas thrust (Fig. 1a; Ahumada and Costa, 2009; Costa et al., 2000). Alluvial fans at the active mountain front have been incised by ephemeral streams that formed several fluvial terraces of Late Pleistocene and Holocene age. We studied these terraces at two sites, the Escondida creek and the Baños Colorados creek (Fig. 1b). At each site four fluvial terraces (T_1 to T_4) are present (Fig. 2). The terraces at both sites are deformed by active faults, which will be described in a separate contribution on the active tectonics of the region.

The sediment in the active streams at both sites has a wide grain size spectrum ranging from silt to boulders with a diameter of up to 2 m. Sediment transport from the internal parts of the Precordillera to the active mountain front (Fig. 3a) occurs mainly by debris flows. The effective sediment transport during such events is illustrated by a recent debris flow that occurred between our two field seasons in August 2008 and August 2009 (Fig. 3b). The debris flow deposited pebbles and cobbles on top of snapped bushes and transported meter-sized boulders. The boulders in the active channels consist of different lithologies exposed in the Precordillera, namely gray Ordovician limestones, greenish Devonian sand- and siltstones, reddish Triassic sandstones and conglomerates, and reddish-orange Miocene sandstones. Boulders consisting of Ordovician and Triassic sediments are present on all terraces, whereas the rapidly weathering and disintegrating boulders of Miocene sandstones decrease in abundance from T_1 to T_2 and are absent on the older terraces T_3 and T_4. Apart from boulders, the terrace deposits consist largely of gravel and sand (Fig. 3c). The surfaces of the older terraces T_3 and T_4 exhibit relatively well developed desert pavements that consist predominantly of pebbles and cobbles and minor amounts of fine-grained sediment in the interstitial space between the larger clasts (Fig. 3d). On the two lower terraces the desert pavement is poorly (T_1) to moderately (T_2) developed and, in contrast to the higher terraces, boulders and clasts on these rather young surfaces show no or only weakly developed desert varnish.

3. Sampling, analytical procedures, and calculation of ^{10}Be exposure ages

To constrain the age of the fluvial terraces we collected samples from flat and pristine parts of four terraces. At site 1 we took samples from terraces T_2 to T_4, whereas at site 2 only terrace T_3 was sampled. In order to compare the different exposure dating approaches outlined in Section 1 we used three different types of samples: boulders, pebbles, and sand. We sampled only Triassic sandstone boulders (Fig. 3e), because they are resistant to weathering, rich in quartz, and widespread on all terraces. All boulders ($n = 18$) had a size of 25 to 50 cm and showed dark desert varnish on their upper surface, except for the five boulders taken from the stream bed of Escondida creek upstream of the terraces. All boulders from the terraces were partly embedded in the terrace deposits, and were therefore in a stable position since their deposition (Fig. 3e).

To apply the amalgamation approach we obtained a sand sample at the surface of each terrace and collected 3–4 subsurface sand samples from pits excavated to a depth of ~180 cm. In addition, one sand sample was taken from the active stream bed of the Escondida creek at site 1 to compare its nuclide concentration with the inherited component present on the terraces. The terrace deposits in all four pits showed clear bedding in the clast and sand horizons. Although shrubs on the terraces may indicate the presence of burrowing animals, we did not recognize any evidence of bioturbation. In the pit on terrace T_3 at site 1 we did find a larger wood sample at a depth of ~20 cm (Fig. 3f). The plant remnant – probably a root or a branch of a

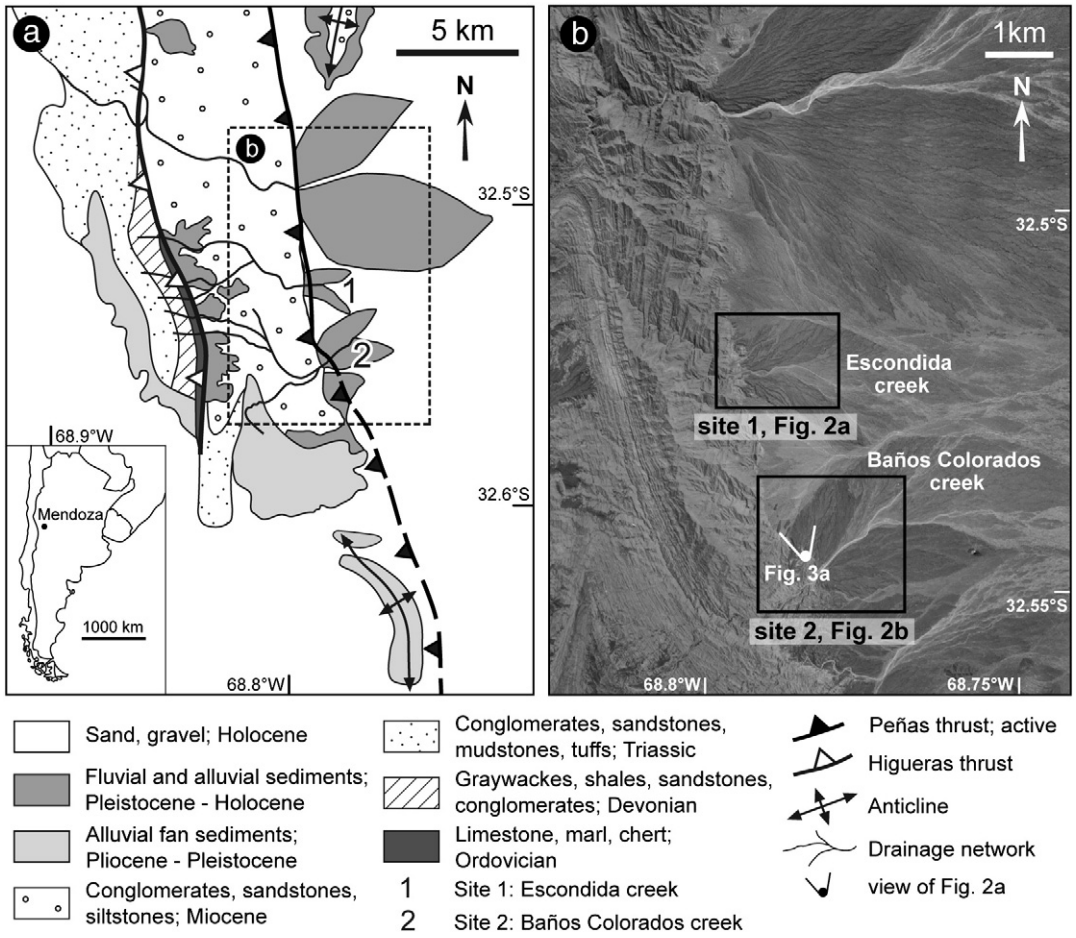

Fig. 1. (a) Geological map of the study area in the Andean Precordillera ca. 40 km north of Mendoza (modified after Ahumada et al., 2006, and Sepúlveda, 2001). (b) Aerial photograph with the two studied sites at Escondida creek and Baños Colorados creek.

bush – had a diameter of 3.5 cm and extended subhorizontally for at least 15 cm, but was broken into numerous parts. It was analyzed for ^{14}C at the Leibniz-Laboratory for Radiometric Dating and Stable Isotope Research in Kiel, Germany (analysis number KIA37376).

The third sample type for ^{10}Be exposure dating were amalgamated pebbles of sandstones from the terraces T_2–T_4 at site 1 (Fig. 3d). For these samples we used exclusively pebbles of Triassic sandstone, i.e. the same lithology as the sampled boulders. Each sample consists of at

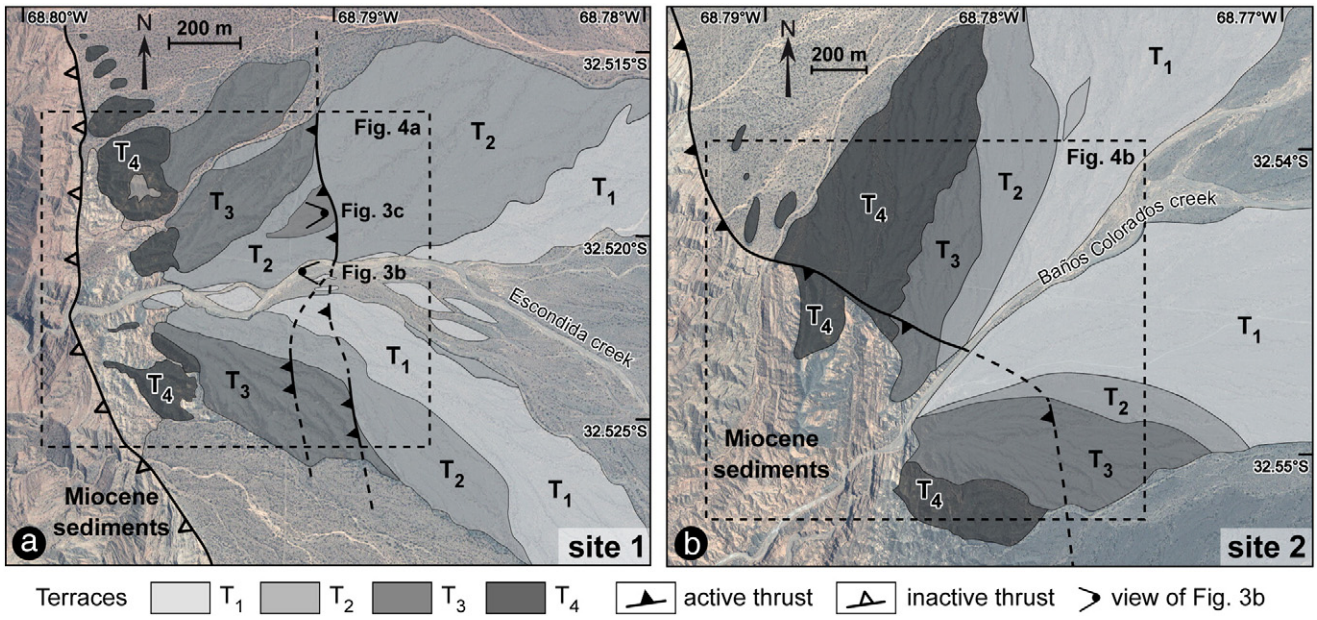

Fig. 2. Geological interpretation of (a) site 1 at the Escondida creek, and (b) site 2 at the Baños Colorados creek.

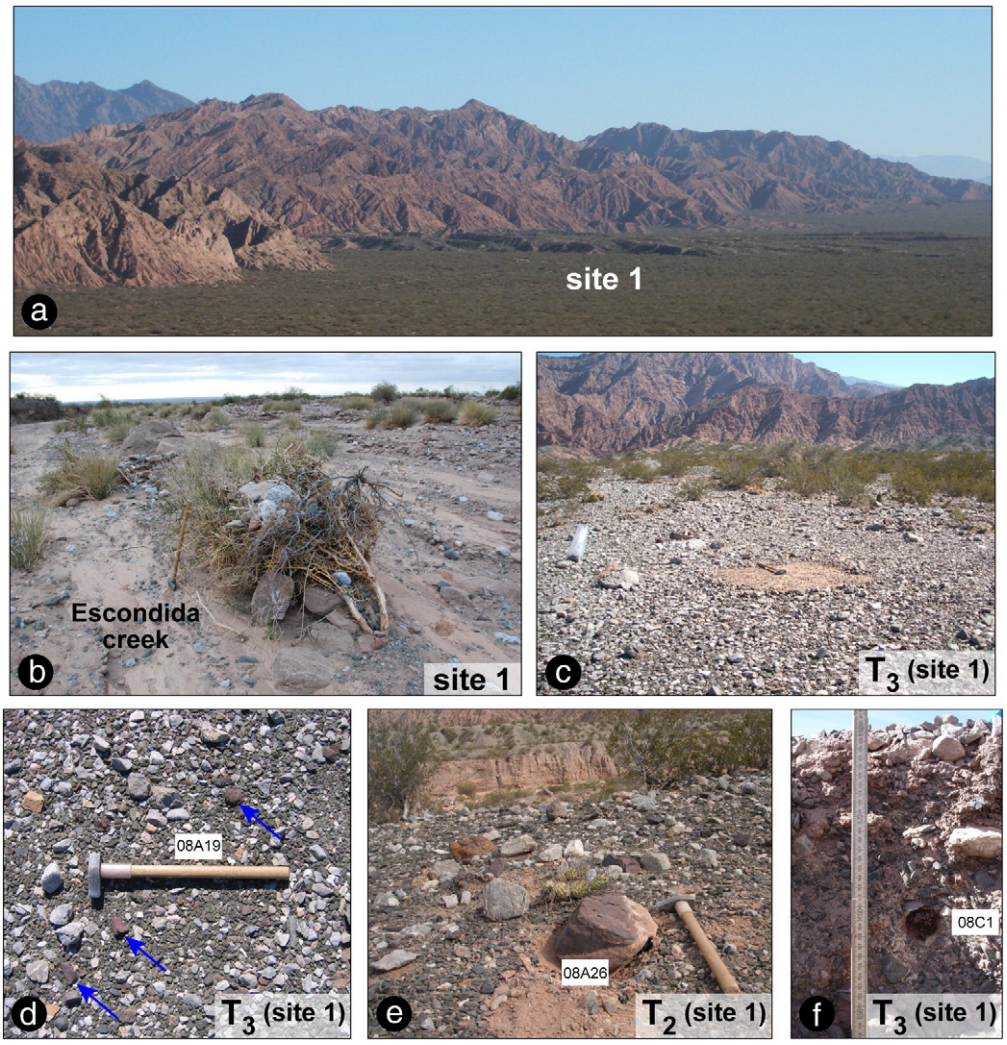

Fig. 3. (a) Northward view along the mountain front of the Precordillera with site 1 (Escondida creek). The point of view is shown in Figure 1b. (b) Boulders deposited in the Escondida creek by a debris flow in the austral summer 2008/2009 which snapped the bush in the center. The point of view is shown in Figure 2a. (c) Terrace T_3 (site 1) viewed towards the west in the direction of the Miocene sandstones. At the smooth square with the hammer we collected the sand sample 08A20 and dug the pit for a depth profile. The point of view is shown in Figure 2a. (d) Desert pavement on T_3 (site 1) at the locality where we took the reddish Triassic sandstone pebbles of sample 08A19. (e) Triassic sandstone boulder on T_2 (site 1). (f) Wood sample obtained from the pit on T_3 (site 1) at a depth of ~20 cm.

least 73 clasts with a length of 1.5–10 cm. Large clasts (4–10 cm) were broken to smaller fragments in order to use a similar amount of material from each clast. Owing to the low abundance of the Triassic pebbles in the excavated pits, it was not possible to amalgamate a reasonable number of pebbles to obtain subsurface samples. Hence, we collected one amalgamated pebble sample in the active river bed of Escondida creek to estimate the average inherited nuclide component of the pebbles.

All rock samples were crushed, washed and sieved, and the 250–500 μm size fraction was split into a magnetic and a non-magnetic fraction. The latter was purified according to procedures introduced by Kohl and Nishiizumi (1992), with 2–4 additional etching steps in aqua regia and HF as described by Goethals et al. (2009). After addition of ~0.26 mg of ^{9}Be carrier solution, the quartz samples (34 to 50 g each) were dissolved and Be was separated in ion exchange columns (for details see Goethals et al., 2009). Finally, the Be was precipitated as $Be(OH)_2$, transformed to BeO and pressed into targets, which were analyzed by accelerator mass spectrometry (AMS) at the ETH Zurich. The measurements were normalized to the standards S555 and S2007 with nominal $^{10}Be/^{9}Be$ ratios of 95.5×10^{-12} and 30.8×10^{-12}, respectively (Kubik and Christl, 2010). These secondary standards were calibrated to the ETH standard material BEST433 (Hofmann et al., 1987). The AMS measurements were carried out as described by Kubik and Christl (2010).

^{10}Be exposure ages were calculated with the CRONUS-Earth ^{10}Be–^{26}Al online calculator, version 2.2.1 (Balco et al., 2008; http://www.hess.ess.washington.edu). The calculator uses a ^{10}Be half-life of 1.387 ± 0.012 Ma (Chmeleff et al., 2010; Korschinek et al., 2010) and corrects for the different half-life and standard material used at the AMS facility in Zurich. We used the time-dependent scaling scheme of Lal (1991) – Stone (2000), which takes temporal variations in the magnetic field intensity into account (Dunai, 2001). The exposure ages of the boulders (Table 1) and amalgamated pebbles (Table 2) were calculated under the assumption of no erosion, since these two sample types consist of resistant Triassic sandstones. To calculate exposure ages from the depth profiles, we first determined the inherited and post-depositional nuclide components of the sand samples, C_i and C_s, using regression analysis. The analysis minimizes the difference between the ^{10}Be concentrations measured in the depth profiles and the exponential function of Eq. (1) and takes the errors of the ^{10}Be concentrations into account. In the regression analysis we used a value of 160 g cm^{-2} for the neutron attenuation length Λ (Gosse and Phillips, 2001) and an estimated density of 2.0 g cm^{-3} for the terrace deposits. This choice results in a value of 0.0125 for the absorption coefficient μ in Eq. (1). As both density and attenuation length are not exactly known we assigned an error of ±10%

Table 1
Geomorphic setting, ^{10}Be concentrations, and apparent ^{10}Be ages of Triassic sandstone boulders.

Sample ID	Geomorphic surface	Latitude WGS84 (°S)	Longitude WGS84 (°W)	Elevation (m)	Shielding factor[a] (−)	Sample thickness[b] (cm)	^{10}Be concentration[c] (10^4 at g^{-1})	^{10}Be age[d] (ka)	Internal 1σ error (ka)	External 1σ error (ka)
Site 1 (Escondida Creek)										
08A24	T_2	32.5210	68.7905	725	0.9992	5	70.2 ± 2.5	**89.9**	± 3.5	± 8.4
08A25	T_2	32.5213	68.7915	733	0.9992	5	75.3 ± 2.7	**96.0**	± 3.9	± 9.0
08A26	T_2	32.5214	68.7920	734	0.9992	5	6.75 ± 0.54	**9.19**	± 0.74	± 1.1
08A1	T_3	32.5198	68.7906	738	0.9991	4	45.6 ± 2.4	**57.3**	± 3.4	± 5.8
08A2	T_3	32.5200	68.7907	737	0.9991	4	64.8 ± 3.7	**81.6**	± 5.2	± 8.5
08A9	T_3	32.5234	68.7936	745	0.9984	4	29.7 ± 1.7	**37.2**	± 2.3	± 3.8
08A10	T_3	32.5236	68.7936	745	0.9984	8	26.6 ± 1.2	**34.7**	± 1.6	± 3.3
08A11	T_3	32.5201	68.7908	735	0.9991	5	14.5 ± 1.1	**19.4**	± 1.5	± 2.2
08A3	T_4	32.5240	68.7955	756	0.9969	4	30.2 ± 1.7	**38.7**	± 2.3	± 4.0
08A29	T_4	32.5241	68.7954	757	0.9969	5	65.6 ± 3.0	**82.1**	± 4.1	± 8.0
08A22	Active stream	32.5120	68.8156	915	–	5	5.79 ± 0.35	**7.42**	± 0.45	± 0.77
09A7	Active stream	32.5233	68.7990	742	–	5	3.60 ± 0.25	**4.99**	± 0.33	± 0.54
09A8	Active stream	32.5234	68.7992	743	–	5	18.71 ± 0.80	**24.4**	± 1.1	± 2.3
09A9	Active stream	32.5234	68.7992	743	–	5	38.8 ± 1.9	**48.0**	± 2.6	± 4.7
09A10	Active stream	32.5221	68.8116	760	–	5	13.18 ± 0.45	**17.3**	± 0.60	± 1.6
Site 2 (Baños Colorados Creek)										
08A4	T_3	32.5472	68.7833	745	0.9997	4	10.75 ± 0.56	**14.31**	± 0.75	± 1.4
08A5	T_3	32.5472	68.7832	743	0.9997	4	14.76 ± 0.63	**19.37**	± 0.84	± 1.8
08A23	T_3	32.5459	68.7829	732	0.9997	5	23.72 ± 0.88	**30.7**	± 1.2	± 2.9

[a] The shielding factor includes only correction for skyline shielding. For boulders from the active stream channel no shielding correction was applied.
[b] To take the sample thickness into account we used a rock density of 2.65 g cm^{-3}.
[c] Blank-corrected ^{10}Be concentrations. The propagated analytical errors (1σ) include the error based on counting statistics and the error of the blank correction.
[d] Ages were calculated under the assumption of no erosion with the CRONUS-Earth ^{10}Be–^{26}Al calculator, version 2.2.1 (Balco et al., 2008; http://www.hess.ess.washington.edu) using the time-dependent scaling scheme of Lal (1991) – Stone (2000). Internal uncertainties include errors from the counting statistics and the blank correction, whereas external uncertainties also include the error of the production rate introduced by the scaling model.

to the absorption coefficient μ. The post-depositional ^{10}Be concentration at the surface, C_s, is reported in Table 2 and was used as input for the online calculator to determine two ages for each depth profile (Table 2). The first age neglects erosion of the terraces and is therefore a *minimum* age. The second age takes erosion into account and was calculated under the assumption of a constant erosion rate of 20 mm ka^{-1}. The choice of this erosion rate is justified in Section 4. All ^{10}Be ages are presented with internal and external errors. Internal errors only take into account the measurement uncertainty and, in case of the depth profiles, a 10% uncertainty on the absorption coefficient μ. They should be used to compare different exposure ages. In contrast, the external errors also include the uncertainty of the local ^{10}Be production rate and are relevant for comparing exposure ages with ages obtained by other methods (Balco et al., 2008).

4. Results of the different dating approaches

The apparent ^{10}Be ages of the boulders from each of the four studied terraces show a large scatter (Fig. 4). For instance, three boulders sampled in a small area of terrace T_3 (site 1) yield apparent ages of 19 ± 2 ka, 57 ± 6 ka, and 82 ± 9 ka, whereas samples from the adjacent lower terrace T_2 range from 9 ± 1 ka to 96 ± 9 ka (Fig. 4a). Furthermore, there is no correlation between apparent ^{10}Be ages and terrace stratigraphy as the two oldest ages of ~90 ka and ~96 ka occur on the youngest sampled terrace T_2 (Fig. 4a). It appears that most, if not all boulders, have a substantial inherited ^{10}Be component that is highly variable from boulder to boulder. This is supported by five boulders that were sampled upstream of the terraces in the active stream bed of the Escondida creek. These boulders have apparent ^{10}Be ages between 5 ka and 48 ka (Table 1).

Compared to boulders, the sand samples from the surfaces of the terraces have much lower ^{10}Be concentrations. Under the assumption of no erosion, the post-depositional nuclide concentrations derived from the depth profiles yield minimum ^{10}Be ages of 3.20 ± 0.48 ka for terrace T_2, 11.1 ± 1.0 ka for T_3, and 16.0 ± 2.6 ka for T_4 (site 1), which are consistent with the stratigraphy of the terraces (Fig. 5a–c, Table 2). Note that the age of terrace T_4 is only based on the three subsurface samples, because the surface sample has a similar ^{10}Be concentration as the sample from a depth of 58 cm (Fig. 5c). Likewise, the uppermost two samples on terrace T_3 at site 2 show similar ^{10}Be concentrations (Fig. 5d). Neglecting the surface sample yields a minimum age of 13.5 ± 1.6 ka, which coincides with the youngest boulder age of 14.31 ± 0.75 ka for this terrace (Fig. 4b).

The presence of variably developed desert pavements on the fluvial terraces indicates that the assumption of no erosion is – strictly speaking – not correct. We interpret these pavements to result from the deflation of fine-grained material, i.e. silt and sand, and the relative enrichment of pebbles at the surface of the terraces (cf. Breed et al., 1997; Cooke and Warren, 1973; Goudie and Wilkinson, 1977). If this interpretation is correct, the progressive enrichment of pebbles in the developing pavements should gradually protect the underlying terrace deposits from further deflation. Thus, it seems plausible that the rate of deflation and erosion slows down during pavement formation. If the pavements had formed rapidly, the *minimum* exposure ages – calculated under the assumption of *no erosion* – may be close to the depositional age of the terraces (Table 2). If, on the other hand, pavement formation has proceeded at low rates and erosion rates have slowly decreased through time, the assumption of a constant erosion rate would be more appropriate for calculating exposure ages. Erosion rates reported for depositional surfaces in different climate regimes range from <1 mm ka^{-1} for glacial outwash surfaces in Patagonia (Hein et al., 2009) and surfaces in the hyperarid Negev desert (Matmon et al., 2009), to ~30 mm ka^{-1} for mid-Pleistocene terraces in humid France (Siame et al., 2004). To take erosion of the studied terraces into account we calculated a second set of ^{10}Be ages using an erosion rate of 20 mm ka^{-1}. The resulting ^{10}Be ages are 0.14 ka (terrace T_2) to 4.1 ka (terrace T_4) older than those determined under the assumption of no erosion (Table 2). The chosen erosion rate of 20 mm ka^{-1} implies that 26 and 40 cm of fine-grained material were removed from the terraces T_3 and T_4, respectively. This

Table 2
Geomorphic setting, ^{10}Be concentrations of amalgamated pebbles and sand samples, and ^{10}Be ages of the terraces.

Sample ID	Sample type[a]	Geomorphic surface	Latitude WGS84 (°S)	Longitude WGS84 (°W)	Elevation (m)	Shielding factor[b] (−)	Sample thickness[c] (cm)	^{10}Be concentration[d] (10^4 at g^{-1})	^{10}Be conc. inher. corr.[e] (10^4 at g^{-1})	^{10}Be age[f,g] (ka)	Internal 1σ error[h] (ka)	External 1σ error[h] (ka)
Site 1 (Escondida creek)												
09A1	Pebbles ($n=73$)	T_2	32.5206	68.7904	725	0.9992	4	11.12 ± 0.56	3.87 ± 0.65	**5.36**	±0.88	±1.0
09A2	Sand (1–4 cm)	T_2	32.5206	68.7904	725	0.9992	–	3.27 ± 0.27	2.30 ± 0.37	**3.20/3.34**	±0.48/±0.52	±0.58/±0.63
09A2a	Sand (43–47 cm)	$T_{2\ depth\ sample}$	"	"	"	–	–	2.61 ± 0.21	–	**–**	–	–
09A2b	Sand (93–97 cm)	$T_{2\ depth\ sample}$	"	"	"	–	–	1.99 ± 0.17	–	**–**	–	–
09A2c	Sand (136–142 cm)	$T_{2\ depth\ sample}$	"	"	"	–	–	1.60 ± 0.15	–	**–**	–	–
09A2d	Sand (176–182 cm)	$T_{2\ depth\ sample}$	"	"	"	–	–	1.40 ± 0.11	–	**–**	–	–
08A19	Pebbles ($n=108$)	T_3	32.5199	68.7904	735	0.9991	3	16.51 ± 0.69	9.26 ± 0.77	**12.4**	±1.0	±1.5
08A20	Sand (1–5 cm)	T_3	32.5199	68.7904	735	0.9991	–	10.13 ± 0.51	8.53 ± 0.78	**11.1/13.0**	±1.0/±1.4	±1.4/±1.9
08A20a	Sand (55–58 cm)	$T_{3\ depth\ sample}$	"	"	"	–	–	6.43 ± 0.40	–	**–**	–	–
08A20b	Sand (110–113 cm)	$T_{3\ depth\ sample}$	"	"	"	–	–	3.69 ± 0.25	–	**–**	–	–
08A20c	Sand (176–182 cm)	$T_{3\ depth\ sample}$	"	"	"	–	–	3.05 ± 0.22	–	**–**	–	–
09A3	Pebbles ($n=115$)	T_4	32.5240	68.7956	758	0.9969	3	21.44 ± 0.87	14.20 ± 0.93	**18.4**	±1.2	±2.0
09A4[g]	Sand (1–4 cm)	T_4	32.5240	68.7956	758	0.9969	–	8.50 ± 0.42	12.59 ± 2.0	**16.0/20.1**	±2.6/±2.9	±4.3/±4.7
09A4a	Sand (57–60 cm)	$T_{4\ depth\ sample}$	"	"	"	–	–	8.21 ± 0.37	–	**–**	–	–
09A4b	Sand (115–120 cm)	$T_{4\ depth\ sample}$	"	"	"	–	–	5.21 ± 0.32	–	**–**	–	–
09A4c	Sand (161–167 cm)	$T_{4\ depth\ sample}$	"	"	"	–	–	3.77 ± 0.24	–	**–**	–	–
08A30	Pebbles ($n=88$)	Active river	32.5221	68.7979	738	–	–	7.24 ± 0.34	–	**–**	–	–
09A5	Sand	Active river	32.5212	68.7899	720	–	–	0.70 ± 0.10	–	**–**	–	–
Site 2 (Baños Colorados creek)												
09A6[g]	Sand (1–4 cm)	T_3	32.5471	68.7833	745	0.9997	–	7.66 ± 0.30	10.4 ± 1.2	**13.5/16.2**	±1.6/±2.4	±2.0/±2.9
09A6a	Sand (59–62 cm)	$T_{3\ depth\ sample}$	"	"	"	–	–	6.89 ± 0.27	–	**–**	–	–
09A6b	Sand (112–118 cm)	$T_{3\ depth\ sample}$	"	"	"	–	–	3.72 ± 0.18	–	**–**	–	–
09A6c	Sand (171–175 cm)	$T_{3\ depth\ sample}$	"	"	"	–	–	3.09 ± 0.17	–	**–**	–	–

[a] For the sand specimens the sampled depth interval is indicated. All pebble samples, which consist of Triassic sandstones, were taken at the surface. The number of pebbles used for each sample is given in parentheses.
[b] The shielding factor includes only correction for skyline shielding.
[c] To take the thickness of the pebble samples into account we used a rock density of 2.65 g cm^{-3}.
[d] Blank-corrected ^{10}Be concentrations. The propagated analytical errors (1σ) include the error based on counting statistics and the error of the blank correction.
[e] ^{10}Be concentrations were corrected for geological inheritance using either the ^{10}Be concentration of the pebbles from the active stream bed or the inherited ^{10}Be concentration derived from the sand samples of the respective depth profiles. The ^{10}Be concentration derived from the depth profiles includes a ± 10% error on the absorption coefficient μ, which is defined as density devided by attenuation length. This concentration is C_s of Eq. (1) and was used as input data for the CRONUS-Earth ^{10}Be–^{26}Al calculator.
[f] Ages were calculated with the CRONUS-Earth ^{10}Be–^{26}Al calculator, version 2.2.1 (Balco et al., 2008; http://www.hess.ess.washington.edu) using the time-dependent scaling scheme of Lal (1991) – Stone (2000). Internal uncertainties include errors from the counting statistics and the blank correction, whereas external uncertanities also include the error of the production rate introduced by the scaling model. The ages of the depth profiles on the left side of the column were calculated under the assumption of no erosion, whereas the ages given on the right side were calculated assuming an erosion rate of 20 mm ka^{-1}.
[g] The ages of the terraces where samples 09A4 and 09A6 were taken are based on the ^{10}Be concentrations of the three subsurface samples as explained in Sections 4 and 5, and the caption to Figure 5.
[h] Errors on the left side of the columns are related to the ages calculated without erosion, whereas errors on the right are related to the ages calculated with an erosion rate of 20 mm ka^{-1}.

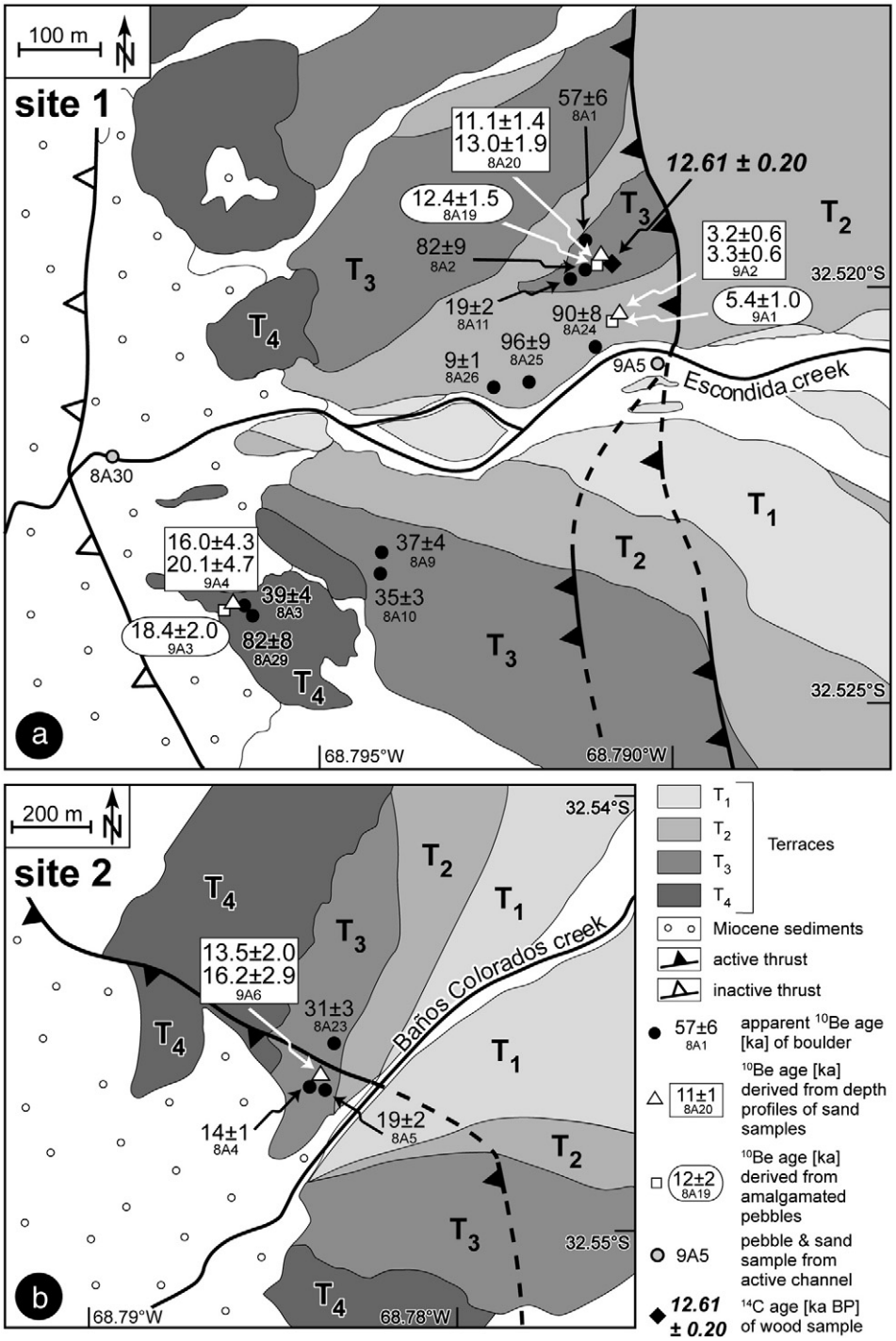

Fig. 4. (a) ^{10}Be exposure ages and one calibrated ^{14}C age at site 1 (Escondida creek). The five boulders from the active channel are not shown because they were taken upstream of the terraces, i.e. west of the area shown in the map. The ages derived from depth profiles on sand were calculated under the assumption of no erosion (ages in the first line) and using a constant erosion rate of 20 mm ka^{-1} (ages in the second line). The 1σ errors of the ^{10}Be ages are given as external uncertainties; whereas the error of the ^{14}C age is given as 2σ uncertainty. (b) ^{10}Be exposure ages at site 2 (Baños Colorados creek).

amount appears to be roughly consistent with the proportion of pebbles observed in the terrace deposits and the generation of the desert pavements by pebble enrichment. Finally, we note that the influx of wind-blown material seems to be unimportant in our study area because a silt layer without pebbles – as present underneath many desert pavements in the western U.S. (McFadden et al., 1987; Wells et al., 1995) – was not observed.

For the pebble samples from the terraces T_2 to T_4 at site 1 the inherited nuclide component was corrected with the ^{10}Be concentration of the pebble sample 08A30 from the active stream bed (Table 2). This approach assumes that the inheritance of pebbles in the active stream is the same as the inheritance of the pebbles on the terraces when they were deposited. Subtracting the ^{10}Be concentration of the stream sediment sample from those of the terrace samples yields ^{10}Be ages of 5.36 ± 0.88 ka for T_2, 12.4 ± 1.0 ka for T_3, and 18.4 ± 1.2 ka for T_4. Considering the 2σ error limits, these ages are consistent with the two sets of ages derived from the depth profiles, which were calculated with and without erosion (Table 2).

The wood sample from the pit on terrace T_3 (site 1) yields a radiocarbon age of 10,620 ± 40 BP, which was calibrated to 12,610 ± 200 calendar years BP (2σ error) using CALIB 5.1 (Stuiver et al., 2009) and the IntCal04 calibration curve (Reimer et al., 2004). The calibrated ^{14}C age of 12.61 ± 0.20 ka BP is in agreement with the ^{10}Be ages for T_3 obtained from the depth profile (11.1 ± 1.4 and 13.0 ± 1.9 ka) and the pebble sample (12.4 ± 1.5 ka) (Table 2).

5. Discussion

The age of the fluvial terraces at the mountain front of the Andean Precordillera north of Mendoza is well constrained by ^{10}Be depth profiles obtained on sand samples and ^{10}Be dating of amalgamated pebbles. Both approaches yield ages that are consistent with the stratigraphy of the terraces and for each surface the ages agree within errors (Table 2). The amalgamated pebbles from terrace T_3 at site 1 yield an age of 12.4 ± 1.5 ka, whereas ages of 11.1 ± 1.4 ka (assuming no erosion) and 13.0 ± 1.9 ka (with an erosion rate of 20 mm ka^{-1}) were obtained from the depth profile. A calibrated ^{14}C age of 12.61 ± 0.20 ka BP for terrace T_3 is consistent with these ^{10}Be ages. On terrace T_4 the age distribution is similar. Here, the pebble sample has an age of 18.4 ± 1.2 ka, which again lies between the two ages derived from the depth profile (16.0 ± 2.6 ka and 20.1 ± 2.9 ka). On the youngest terrace T_2 the nominal age of the pebbles is older than those obtained from the depth profile, although the three ages agree within 2σ errors (Table 2).

Although the exposure ages derived from depth profiles and amalgamated pebbles yield consistent results, both dating approaches have inherent weaknesses. By using pebbles from the active stream bed to correct for the inherited nuclide component, one assumes that their mean ^{10}Be concentration is identical to those of the terrace pebbles. As this assumption is not necessarily correct, the ages of the amalgamated pebbles have an additional uncertainty that is difficult to quantify. For the sand samples from depth profiles, *minimum* exposure ages calculated by neglecting erosion may only provide useful lower limits, if pavement formation by deflation has occurred rapidly. The presence of desert pavements indicates that erosion should be taken into account, however, choosing an appropriate erosion rate is difficult because pavement formation is most likely a non-linear process. The observation that the age of ~13.0 ka for terrace T_3 (calculated with erosion) agrees well with the ^{14}C age of 12.6 ka suggests that the chosen erosion rate of 20 mm ka^{-1} is roughly adequate for terrace T_3. If erosion by deflation of fine-grained material has decelerated through time, the ^{10}Be age for terrace T_4 may be slightly overestimated because both T_3 and T_4 possess rather well developed pavements. On the other hand, the age of terrace T_2 that considers erosion may be slightly too young, if deflation proceeded rapidly during the initial stage of pavement formation. This would explain why the nominal age of the pebbles from T_2 is older than the age obtained from the depth profile (Table 2). These considerations suggest that the youngest and oldest exposure ages derived from pebble and sand samples represent reasonable lower and upper bounds for the depositional age of the fluvial terraces. Thus, we infer that the terraces at site 1 formed at 3–5 ka (terrace T_2), 11–13 ka (terrace T_3), and 16–20 ka (terrace T_4), while terrace T_3 at site 2 is 13–16 ka old.

The ^{10}Be profiles in all four pits show decreasing ^{10}Be concentrations with depth, but in profiles on T_4 (site 1) and T_3 (site 2) the surface samples and that from a depth of ~60 cm have similar nuclide concentrations (Fig. 5c,d). Hence, the surface samples have ^{10}Be concentrations that are too low compared to the depth samples and we neglected them when calculating the ^{10}Be ages. The phenomenon of a too low ^{10}Be concentration in sand surface samples was already mentioned by Matmon et al. (2006) on fluvial samples from southern California. The low ^{10}Be concentrations of the surface samples is difficult to explain because bedding is preserved at the pit walls and there is no clear evidence for bioturbation. Still, the former presence of bushes at the sampled sites may have caused local mixing in small parts of the pits that did not affect the sections exposed in the pit walls. Another process that may have contributed to a lowering of the ^{10}Be concentration of the surface samples is the disaggregation of boulders composed of Miocene sandstone. This boulder type is

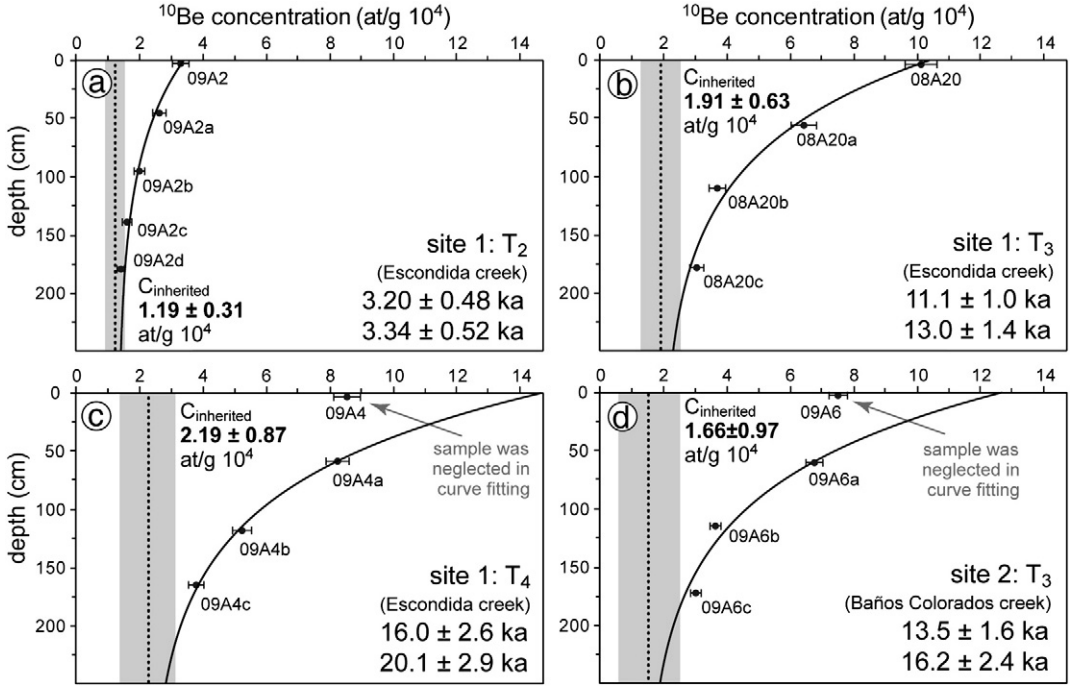

Fig. 5. ^{10}Be depth profiles derived from sand samples at site 1 (a–c) and at site 2 (d). The dotted vertical line represents the inherited ^{10}Be concentration and the gray field indicates its 1σ error. The post-depositional ^{10}Be concentration at the surface, C_s, determines the age of the terraces and is given in Table 2. Errors of the ages (1σ) are given as internal uncertainties. Ages in the first line were calculated under the assumption of no erosion, whereas the ones in the second line assume an erosion rate of 20 mm ka^{-1}. In the pit on terrace T_3 (b) a calibrated ^{14}C age of 12.61 ± 0.20 ka BP obtained from a wood sample confirms the ^{10}Be age of the terrace.

abundant on terrace T_1 but rapidly weathering and disintegrating, and therefore does not occur on terraces T_3 and T_4. The decay of such boulders on the older terraces likely produces sand grains with low ^{10}Be concentrations, but the former positions of these boulders are difficult to recognize. If we had sampled areas where such boulders were once present this would help to explain the low ^{10}Be concentrations of the two surface samples.

The nominal values for the pre-depositional ^{10}Be concentration obtained from the depth profiles at site 1 slightly decrease with terrace age from ~2.2 to ~1.2×10^4 at g^{-1} (Fig. 5a–c). Although the different values agree within error, this may indicate a trend towards a lower inheritance for younger surfaces. This is supported by the even lower ^{10}Be concentration of ~0.7×10^4 at g^{-1} of the sand sample from the active stream bed of Escondida creek (Table 2). The low ^{10}Be concentration of this sample emphasizes that for determining precise exposure ages the inherited component should be quantified from depth profiles on each surface to be dated.

Although reasonable exposure ages for depositional surfaces have been obtained by dating individual cobbles or boulders (e.g. Brown et al., 2002; Kirby et al., 2006; Mériaux et al., 2009; Palumbo et al., 2009; van der Woerd et al., 1998; Zehfuss et al., 2001), the highly variable ^{10}Be ages of all boulders analyzed in this study demonstrate that the approach may fail completely. As all analyzed boulders consist of resistant Triassic sandstone, the huge differences in their apparent ages (Table 1) cannot result from differences in the erosion of the boulders after their deposition. The variable ^{10}Be ages must be caused by a variable and significant inherited nuclide component, which is also present in the five boulders from the active stream bed (Table 1). Note that these boulders were sampled 0.2 to 2 km upstream of the four terraces at site 1. In principal, two scenarios are possible to explain this phenomenon. First, the individual sandstone boulders may have experienced different irradiation histories during their exhumation in the source area, which is located west of the Higueras thrust (Fig. 1a), and during sedimentary transport to the mountain front through the channel system. It is unlikely that the boulders acquired their high ^{10}Be concentration during sedimentary transport, because their transport occurs largely via debris flows (Fig. 3b). If, on the other hand, the boulders acquired their pre-depositional component during exhumation, we would expect similar nuclide concentrations in boulders and pebbles, because both consist of Triassic sandstones. As the average pre-depositional ^{10}Be concentration of the boulders (which is equivalent to ~30 ka of exposure) is three times higher than that of the amalgamated pebbles (equivalent to ~10 ka of exposure), this is clearly not the case. Hence, we favour a second scenario and propose that the high and variable inheritance of the boulders is related to their temporal storage and irradiation on the way to the mountain front. In the internal part of the Precordillera several alluvial fans are aligned in the footwall of the presently inactive Higueras thrust (Fig. 1a). We argue that the boulders have been irradiated there and were later reworked and transported to the studied terraces at the active mountain front. We envisage that the remobilization of boulders from the eroding alluvial fans is more difficult than that of smaller clasts, which would explain the higher pre-depositional ^{10}Be concentrations of the boulders as compared to the pebbles.

Geological and geomorphological studies demonstrate that the oscillatory filling and excavation of intramontane basins as a result of climatic changes has played an important role during the evolution of the eastern Andes (Beer et al., 1990; Hilley and Strecker, 2005; Kleinert and Strecker, 2001). Hence, exposure and irradiation of sediment temporally stored in intramontane basins may have been a common process during the formation of the Andean fold-and-thrust belt. As a consequence, the presence of a high and variable pre-depositional nuclide component may be the rule rather than the exception at the mountain front of the eastern Andes. In other regions exposure dating of depositional surfaces has also been hampered by a variable inheritance of cobbles and pebbles. For instance, a study at the northern margin of Tibet revealed that seven out of ten individual cobbles from an active stream channel had ^{10}Be and ^{26}Al concentrations equivalent to exposure periods of 2.4 to 60 ka (Mériaux et al., 2005). Likewise, ten boulders from an active stream in California yielded significant and variable ^{10}Be concentrations of 0.09 to 1.96×10^5 at g^{-1} (Matmon et al., 2005). Another example from an arid region in Israel on fluvial sediments showed that all out of four analyzed boulders yielded apparent ages that exceed the depositional age of the fluvial terraces by tens of thousands of years (Guralnik et al., 2011). In central Iran single cobbles and amalgamated pebbles from two tectonically offset alluvial surfaces yielded ^{10}Be ages that vary from 18 to 65 ka and from 22 to 78 ka, respectively, whereas four cobbles from the active river bed had ^{10}Be concentrations equivalent to 6–18 ka of exposure (Le Dortz et al., 2009). The variable ^{10}Be concentrations of the amalgamated pebbles was most likely caused by the small number of only ten pebbles which were amalgamated per sample.

Given the problem that may be caused by the temporal deposition and subsequent remobilization of boulders, an alternative approach of dating alluvial surfaces is to analyze depth profiles in order to quantify the pre-depositional nuclide component (Braucher et al., 2009; Hein et al., 2009; Schaller et al., 2010). An important prerequisite for applying this approach is the relatively rapid deposition of sediment with a uniform inheritance and a thickness of at least ~1.5 m. The gradually decreasing ^{10}Be concentration in all our pits indicates that fluvial sediment with a thickness of at least 1.7–1.8 m was indeed deposited during formation of the different terraces (Fig. 5). Another problem that may be encountered when applying depth profiles is that the number of suitable pebbles or cobbles from a single lithology is too small. As a result, the averaging of the inherited nuclide component of individually clasts is not assured and the depth profiles may not show an exponential decrease of the nuclide concentrations with depth. Therefore, sand samples composed of a large number of grains are better suited to constrain the pre-depositional nuclide component than are samples consisting of a limited number of amalgamated pebbles – as already documented by Perg et al. (2001), Phillips et al. (1998), and Schaller et al. (2010).

6. Conclusions

We have applied three different approaches to date fluvial terraces at the active mountain front of the Andes using *in situ*-produced ^{10}Be in quartz. Amalgamated samples of sand and pebbles yield consistent exposure ages that have been corrected for an inherited nuclide component. In contrast, all boulders except one contain such a high and variable pre-depositional component that it is impossible to determine the age of the terraces from their apparent ^{10}Be ages. Hence, in this study the determination of precise exposure ages relies on the quantification of the inherited component using sand samples from depth profiles and pebbles from an active stream. The inherited ^{10}Be concentration in the amalgamated pebble samples is about four times higher than that of the sand, which is related to their different source areas and transport histories. The sand is largely derived from soft and rapidly weathering Miocene sediments, which are exposed near the active mountain front. In contrast, the pebbles (and boulders) originate from resistant Triassic sandstones in the internal part of the mountain chain and have a different exhumation and transport history, including a period of intermittent storage.

In general, each of the three different exposure dating approaches has his merits and pitfalls. If boulders do not contain a significant inherited component and consist of resistant lithologies, they may yield tightly clustered exposure ages, which is often the case for moraines. Dating of amalgamated pebbles has the advantage that pebbles are easy to collect, although mixing of different lithologies should be avoided because each lithology may have a distinct mean

inheritance. Unfortunately, the low abundance of pebbles often prevents the sampling of a sufficient number of pebbles in depth profiles. This hinders the determination of the inherited component, although pebble samples taken in active streams may alleviate this problem. When dating relatively young depositional surfaces that have experienced only minor erosion, the inherited component may be precisely determined with sand samples from depth profiles. This approach may yield accurate exposure ages if bioturbation has not disturbed the uppermost decimeters of the alluvial deposits.

Acknowledgements

We thank Anne Niehus for her help in the lab, Veronica Rapelius for ICP analyzes of leached quartz separates, and Peter Kubik for the measurement of the ^{10}Be concentrations. Furthermore, we thank three anonymous referees for their careful and constructive reviews, which helped us to improve the manuscript, and Mark Harrison for editorial handling of the manuscript. Funding of this project by the German Research Foundation (DFG; grant no. HE 1704/6-1) is gratefully acknowledged.

References

Ahumada, E.A., Costa, C.H., 2009. Antithetic linkage between oblique Quaternary thrusts at the Andean front, Argentine Precordillera. J. South Am. Earth Sci. 28, 207–216.

Ahumada, E., Costa, C.H., Gardini, C.E., Diederix, H., 2006. La estructura del extremo sur de la Sierra de Las Peñas-Las Higueras, Precordillera de Mendoza. Assoc. Geol. Arg. 6, 11–17 (in Spanish).

Anderson, R.S., Repka, J.L., Dick, G.S., 1996. Explicit treatment of inheritance in dating depositional surfaces using in situ ^{10}Be and ^{26}Al. Geology 24, 47–51.

Balco, G., Stone, J.O., Lifton, N.A., Dunai, T.J., 2008. A complete and easily accessible means of calculating surface exposure ages or erosion rates from ^{10}Be and ^{26}Al measurements. Quat. Geochron. 3, 174–195.

Beer, J.A., Allmendinger, R.W., Figueroa, D.E., Jordan, T.E., 1990. Seismic stratigraphy of a Neogene piggyback basin, Argentina. Am. Assoc. Petrol. Geol. Bull. 74, 1183–1202.

Bierman, P.R., Gillespie, A.R., Caffee, M.W., 1995. Cosmogenic ages for earthquake recurrence intervals and debris flow fan deposition, Owens Valley, California. Science 270, 447–450.

Braucher, R., Del Castillo, P., Siame, L., Hidy, A.J., Bourlès, D.L., 2009. Determination of both exposure time and denudation rate from an in situ-produced ^{10}Be depth profile: a mathematical proof of uniqueness. Model sensitivity and applications to natural cases. Quat. Geochron. 4, 56–67.

Breed, C.S., McCauley, J.F., Whitney, M.I., 1997. Wind erosion forms. In: Thomas, D. (Ed.), Arid zone Geomorphology. Belhaven Press, London, pp. 437–464.

Brown, E.T., Bendick, R., Bourlès, D.L., Gaur, V., Molnar, P., Raisbeck, G.M., Yiou, F., 2002. Slip rates of the Karakorum fault, Ladakh, India, determined using cosmic ray exposure dating of debris flows and moraines. J. Geophys. Res. 107 (B9), 2192.

Burbank, D., Meigs, A., Brozovic, N., 1996. Interactions of growing folds and coeval depositional systems. Basin Res. 8, 199–223.

Chmeleff, J., von Blanckenburg, F., Kossert, K., Jakob, D., 2010. Determination of the ^{10}Be half-life by multicollector ICP-MS and liquid scintillation counting. Nucl. Instr. Meth. B 268, 192–199.

Cooke, R.U., Warren, A., 1973. Geomorphology in Deserts. Batsford, London.

Costa, C.H., Gardini, C.E., Diederix, H., Cortés, J.M., 2000. The Andean orogenic front at Sierra de Las Peñas-Las Higueras, Mendoza, Argentina. J. South Am. Earth Sci. 13, 287–292.

Dühnforth, M., Densmore, A.L., Ivy-Ochs, S., Allen, P.A., Kubik, P.W., 2007. Timing and patterns of debris flow deposition on Shepherd and Symmes creek fans, Owens Valley, California, deduced from cosmogenic ^{10}Be. J. Geophys. Res. 112, F03S15. doi:10.1029/2006JF000562.

Dunai, T.J., 2001. Influence of secular variation of the geomagnetic field on production rates of in situ produced cosmogenic nuclides. Earth Planet. Sci. Lett. 193, 197–212.

Goethals, M.M., Hetzel, R., Niedermann, S., Wittmann, H., Fenton, C.R., Kubik, P.W., Christl, M., von Blanckenburg, F., 2009. An improved experimental determination of cosmogenic ^{10}Be/^{21}Ne and ^{26}Al/^{21}Ne production ratios in quartz. Earth Planet. Sci. Lett. 284, 187–198.

Gold, R.D., Cowgill, E., Arrowsmith, J.R., Gosse, J., Chen, X., Wang, X.-F., 2009. Riser diachroneity, lateral erosion, and uncertainty in rates of strikeslip faulting: a case study from Tuzidun along the Altyn Tagh Fault, NW China. J. Geophys. Res. 114, B04401. doi:10.1029/2008JB005913.

Gosse, J.C., Phillips, F.M., 2001. Terrestrial in situ cosmogenic nuclides: theory and application. Quat. Sci. Rev. 20, 1475–1560.

Goudie, A.S., Wilkinson, J., 1977. The Warm Desert Environment. Cambridge University Press, Cambridge.

Guralnik, B., Matmon, A., Avni, Y., Porat, N., Fink, D., 2011. Constraining the evolution of river terraces with integrated OSL and cosmogenic nuclide data. Quat. Geochron. 6, 22–32.

Hancock, G.S., Anderson, R.S., Chadwick, O.A., Finkel, R.C., 1999. Dating fluvial terraces with ^{10}Be and ^{26}Al profiles: application to the Wind River, Wyoming. Geomorphology 27, 41–60.

Hein, A.S., Hulton, N.R.J., Dunai, T.J., Schnabel, C., Kaplan, M.R., Naylor, M., Xu, S., 2009. Middle Pleistocene glaciation in Patagonia dated by cosmogenic-nuclide measurements on outwash gravels. Earth Planet. Sci. Lett. 286, 184–197.

Hetzel, R., Niedermann, S., Tao, M.X., Kubik, P.W., Ivy-Ochs, S., Gao, B., Strecker, M.R., 2002. Low slip rates and long-term preservation of geomorphic features in Central Asia. Nature 417, 428–432.

Hetzel, R., Niedermann, S., Tao, M.X., Kubik, P.W., Strecker, M.R., 2006. Climatic versus tectonic control on river incision at the margin of NE Tibet: ^{10}Be exposure dating of river terraces at the mountain front of the Qilian Shan. J. Geophys. Res. 111, F03012. doi:10.1029/2005JF000352.

Hilley, G.E., Strecker, M.R., 2005. Processes of oscillatory basin filling and excavation in a tectonically active orogen: Quebrada del Toro Basin, NW Argentina. Geol. Soc. Am. Bull. 117, 887–901.

Hofmann, H., Beer, J., Bonani, G., von Gunten, H.R., Raman, S., Suter, M., Walker, R.L., Wölfli, W., Zimmermann, D., 1987. ^{10}Be: half-life and AMS standards. Nucl. Instr. Meth. B 29, 32–36.

Kaplan, M.R., Schaefer, J.M., Denton, G.H., Barrell, D.J.A., Chinn, T.J.H., Putnam, A.E., Andersen, B.G., Finkel, R.C., Schwartz, R., Doughty, A.M., 2010. Glacier retreat in New Zealand during the Younger Dryas stadial. Nature 467, 194–197.

Kirby, E., Burbank, D.W., Reheis, M., Phillips, F., 2006. Temporal variations in slip rate of the White Mountain Fault Zone, Eastern California. Earth Planet. Sci. Lett. 248, 168–185.

Kleinert, K., Strecker, M.R., 2001. Climate change in response to orographic barrier uplift: Paleosol and stable isotope evidence from the late Neogene Santa María basin, northwestern Argentina. Geol. Soc. Am. Bull. 113, 728–742.

Kohl, C.P., Nishiizumi, K., 1992. Chemical isolation of quartz for measurement of in-situ-produced cosmogenic nuclides. Geochim. Cosmochim. Acta 56, 3583–3587.

Korschinek, G., Bergmaier, A., Faestermann, T., Gerstmann, U.C., Knie, K., Rugel, G., Wallner, A., Dillmann, I., Dollinger, G., von Gostomski, C.L., Kossert, K., Maiti, M., Poutivtsev, M., Remmert, A., 2010. A new value for the half-life of ^{10}Be by Heavy-Ion Elastic Recoil Detection and liquid scintillation counting. Nucl. Instr. Meth. B 268, 187–191.

Kubik, P.W., Christl, M., 2010. ^{10}Be and ^{26}Al measurements at the Zurich 6 MV Tandem AMS facility. Nucl. Instr. Meth. B 268, 880–883.

Lal, D., 1991. Cosmic ray labeling of erosion surfaces: in situ nuclide production rates and erosion models. Earth Planet. Sci. Lett. 104, 424–439.

Le Dortz, K., Meyer, B., Sébrier, M., Nazari, H., Braucher, R., Fattahi, M., Benedetti, L., Foroutan, M., Siame, L., Bourlès, D., Talebian, M., Bateman, M.D., Ghoraishi, M., 2009. Holocene right-slip rate determined by cosmogenic and OSL dating on the Anar fault, Central Iran. Geophys. J. Int. 179, 700–710.

Matmon, A., Schwartz, D.P., Finkel, R., Clemmens, S., Hanks, T., 2005. Dating offset fans along the Mojave section of the San Andreas fault using cosmogenic ^{26}Al and ^{10}Be. Geol. Soc. Am. Bull. 117, 795–807.

Matmon, A., Nichols, K., Finkel, R., 2006. Isotopic insights into smoothening of abandoned fan surfaces, southern California. Quat. Res. 66, 109–118.

Matmon, A., Simhai, O., Amit, R., Haviv, I., Porat, N., McDonald, E., Benedetti, L., Finkel, R., 2009. Desert pavement-coated surfaces in extreme deserts present the longest-lived landforms on Earth. Geol. Soc. Am. Bull. 121, 688–697.

McFadden, L.D., Wells, S.G., Jercinovich, M.J., 1987. Influences of eolian and pedogenic processes on the origin and evolution of desert pavements. Geology 15, 504–508.

Mériaux, A.-S., Tapponnier, P., Ryerson, F.J., Xu, X.W., King, G., van der Woerd, J., Finkel, R.C., Li, H.B., Caffee, M.W., Xu, Z.Q., Chen, W.B., 2005. The Aksay segment of the northern Altyn Tagh fault: tectonic geomorphology, landscape evolution, and Holocene slip rate. J. Geophys. Res. 110, B04404. doi:10.1029/2004JB003210.

Mériaux, A.-S., Sieh, K., Finkel, R.C., Rubin, C.M., Taylor, M.H., Meltzner, A.J., Ryerson, F.J., 2009. Kinematic behavior of southern Alaska constrained by westward decreasing postglacial slip rates on the Denali Fault, Alaska. J. Geophys. Res. 114, B03404. doi:10.1029/2007JB005053.

Meyer, H., Hetzel, R., Strauss, H., 2010. Erosion rates on different timescales derived from cosmogenic ^{10}Be and river loads: implications for landscape evolution in the Rhenish Massif, Germany. Int. J. Earth Sci. 99, 395–412.

Palumbo, L., Hetzel, R., Tao, M., Li, X., Guo, J., 2009. Deciphering the rate of mountain growth during topographic pre-steady state: an example from the NE margin of the Tibetan Plateau. Tectonics 28 TC4017.

Perg, L.A., Anderson, R.S., Finkel, R.C., 2001. Use of a new ^{10}Be and ^{26}Al inventory method to date marine terraces, Santa Cruz, California, USA. Geology 29, 879–882.

Phillips, F.M., Zreda, M.G., Gosse, J.C., Klein, J., Evenson, E.B., Hall, R.D., Chadwick, O.A., Sharma, P., 1997. Cosmogenic ^{36}Cl and ^{10}Be ages of Quaternary glacial and fluvial deposits of the Wind River Range, Wyoming. Geol. Soc. Am. Bull. 109, 1453–1463.

Phillips, W.M., McDonald, E.V., Reneau, S.L., Poths, J., 1998. Dating soils and alluvium with cosmogenic ^{21}Ne depth profiles: case studies from the Pajarito Plateau, New Mexico, USA. Earth Planet. Sci. Lett. 160, 209–223.

Pratt, B., Burbank, D.W., Heimsath, A., Ojha, T., 2002. Impulsive alluviation during early Holocene strengthened monsoons, central Nepal Himalaya. Geology 30, 911–914.

Ramos, V.A., Cristallini, E.O., Pérez, D.J., 2002. The Pampean flat-slab of the Central Andes. J. South Am. Earth Sci. 15, 59–78.

Reimer, P.J., Baillie, M.G.L., Bard, E., Bayliss, A., Beck, J.W., Bertrand, C.J.H., Blackwell, P.G., Buck, C.E., Burr, G.S., Cutler, K.B., Damon, P.E., Edwards, R.L., Fairbanks, R.G., Friedrich, M., Guilderson, T.P., Hogg, A.G., Hughen, K.A., Kromer, B., McCormac, G., Manning, S., Ramsey, C.B., Reimer, R.W., Remmele, S., Southon, J.R., Stuiver, M., Talamo, S., Taylor, F.W., van der Plicht, J., Weyhenmeyer, C.E., 2004. IntCal04 terrestrial radiocarbon age calibration, 0–26 cal kyr BP. Radiocarbon 46, 1029–1058.

Repka, J.L., Anderson, R.S., Finkel, R.C., 1997. Cosmogenic dating of fluvial terraces, Fremont River, Utah. Earth Planet. Sci. Lett. 152, 59–73.

Ritz, J.F., Bourlès, D., Brown, E.T., Carretier, S., Chéry, J., Enhtuvshin, B., Galsan, P., Finkel, R.C., Hanks, T.C., Kendrick, K.J., Philip, H., Raisbeck, G., Schlupp, A., Schwartz, D.P., Yiou, F., 2003. Late Pleistocene to Holocene slip rates for the Gurvan Bulag thrust fault (Gobi-Altay, Mongolia) estimated with ^{10}Be dates. J. Geophys. Res. 108 (B3), 2162. doi:10.1029/2001JB000553.

Schaefer, J.M., Denton, G.H., Kaplan, M., Putnam, A., Finkel, R.C., Barrell, D.J.A., Andersen, B.G., Schwartz, R., Mackintosh, A., Chinn, T., Schlüchter, C., 2009. High-frequency Holocene glacier fluctuations in New Zealand differ from the northern signature. Science 324, 622–625.

Schaller, M., von Blanckenburg, F., Hovius, N., Veldkamp, A., van den Berg, M.W., Kubik, P.W., 2004. Paleoerosion rates from cosmogenic ^{10}Be in a 1.3 Ma terrace sequence: response of the river Meuse to changes in climate and rock uplift. J. Geol. 112, 127–144.

Schaller, M., Ehlers, T.A., Blum, J.D., 2010. Soil transport on a moraine foreslope. Geomorphology 115, 117–128.

Sepúlveda, E., 2001. Hoja Geológica 3369-II, Mendoza. Provincias de Mendoza y San Juan. Instituto de Geología y Recursos Minerales, Servicio Geológico Minero Argentino, Boletín 252, Buenos Aires (in Spanish).

Siame, L.L., Bourlès, D.L., Sébrier, M., Bellier, O., Castano, J.C., Araujo, M., Perez, M., Raisbeck, G.M., Yiou, F., 1997. Cosmogenic dating ranging from 20 to 700 ka of a series of alluvial fan surfaces affected by the El Tigre fault, Argentina. Geology 25, 975–978.

Siame, L., Bellier, O., Braucher, R., Sébrier, M., Cushing, M., Bourlès, D., Hamelin, B., Baroux, E., de Voogd, B., Raisbeck, G., Yiou, F., 2004. Local erosion rates versus active tectonics: cosmic ray exposure modelling in Provence (south-east France). Earth Planet. Sci. Lett. 220, 345–364.

Stone, J.O., 2000. Air pressure and cosmogenic isotope production. J. Geophys. Res. 105, 23753–23759.

Stuiver, M., Reimer, P.J., Reimer, R., 2009. CALIB Radiocarbon Calibration. http://www.radiocarbon.pa.qub.ac.uk/calib (accessed February 2009).

van der Woerd, J., Ryerson, F.J., Tapponnier, P., Gaudemer, Y., Finkel, R., Mériaux, A.-S., Caffee, M., Zhao, G.G., He, Q.L., 1998. Holocene left-slip rate determined by cosmogenic surface dating on the Xidatan segment of the Kunlun fault (Qinghai, China). Geology 26, 695–698.

van der Woerd, J., Klinger, Y., Sieh, K., Tapponnier, P., Ryerson, F.J., Mériaux, A.-S., 2006. Long-term slip rate of the southern San Andreas Fault from ^{10}Be - ^{26}Al surface exposure dating of an offset alluvial fan. J. Geophys. Res. 111, B04407. doi:10.1029/2004JB003559.

Vergés, J., Ramos, V.A., Meigs, A., Cristallini, E., Bettini, F.H., Cortés, J.M., 2007. Crustal wedging triggering recent deformation in the Andean thrust front between 31°S and 33°S: Sierras Pampeanas–Precordillera interaction. J. Geophys. Res. 112, B03S15. doi:10.1029/2006JB004287.

Wells, S.G., McFadden, L.D., Poths, J., Olinger, C.T., 1995. Cosmogenic ^{3}He surface-exposure dating of stone pavements: Implications for landscape evolution in deserts. Geology 23, 613–616.

Zehfuss, P.H., Bierman, P.R., Gillespie, A.R., Burke, R.M., Caffee, M.W., 2001. Slip rates on the Fish Springs fault, Owens Valley, California, deduced from cosmogenic ^{10}Be and ^{26}Al and soil development on fan surfaces. Geol. Soc. Am. Bull. 113, 241–255.